Acta Crystallographica Section D
**Biological Crystallography**
ISSN 1399-0047

# The multiple nucleotide–divalent cation binding modes of *Saccharomyces cerevisiae* CK2$\alpha$ indicate a possible co-substrate hydrolysis product (ADP/GDP) release pathway

**Huihui Liu,[a,b] Hong Wang,[a,b] Maikun Teng[a,b]* and Xu Li[a,b]***

[a]School of Life Sciences, University of Science and Technology of China, 96 Jinzhai Road, Hefei, Anhui 230026, People's Republic of China, and [b]Key Laboratory of Structural Biology, Chinese Academy of Sciences, 96 Jinzhai Road, Hefei, Anhui 230026, People's Republic of China

Correspondence e-mail: mkteng@ustc.edu.cn, sachem@ustc.edu.cn

Received 12 August 2013
Accepted 10 October 2013

**PDB references:** *sc*CK2$\alpha$–ATP–$Mg^{2+}$, 4mwh; *sc*CK2$\alpha$–AMPPN, 4jqe; *sc*CK2$\alpha$–GMPPNP–$Mg^{2+}$, 4jr7; *sc*K2$\alpha$–GMPPNP–$Mn^{2+}$, 4lfi

CK2 is a ubiquitous and conserved protein kinase in eukaryotic organisms and is important in many biological processes. It is unique in maintaining constitutive activity and in using both ATP and GTP as phosphor donors. In this study, crystal structures of recombinant *Saccharomyces cerevisiae* CK2$\alpha$ (*sc*CK2$\alpha$) complexed with GMPPNP, ATP and AMPPN with either $Mg^{2+}$ or $Mn^{2+}$ as the coordinated divalent cation are presented. The overall structure of *sc*CK2$\alpha$ shows high similarity to its homologous proteins by consisting of two domains with the co-substrate lying in the cleft between them. However, three characteristic features distinguish *sc*CK2$\alpha$ from its homologues. Firstly, the Lys45–Glu53 and Arg48–Glu53 interactions in *sc*CK2$\alpha$ lead Lys50 to adopt a unique conformation that is able to stabilize the $\gamma$-phosphate of the co-substrate, which makes the existence of the 'essential divalent cation' not so essential. The multiple nucleotide–divalent cation binding modes of the active site of *sc*CK2$\alpha$ are apparently different from the two-divalent-cation-occupied active site of *Zea mays* CK2$\alpha$ and human CK2$\alpha$. Secondly, conformational change of Glu53 in *sc*CK2$\alpha$–AMPPN breaks its interaction with Lys45 and Arg48; as a result, the co-substrate binding pocket becomes more open. This may suggest a clue to a possible ADP/GDP-release pathway, because the NE1 atom of the Trp in the 'DWG motif' of CK2$\alpha$ forms a hydrogen bond to the O atom of Leu212, which seems to make ADP release by means of the 'DFG-in flip to DFG-out' model found in most eukaryotic protein kinases impossible. Coincidentally, two sulfate ions which may mimic two phosphate groups were captured by Arg161 and Lys197 around the pocket. Mutagenesis and biochemical experiments on R161A and K197A mutants support the above proposal. Finally, *sc*CK2$\alpha$ is unique in containing an insertion region whose function had not been identified in previous research. It is found that the insertion region contributes to maintaining the constitutively active conformation of the *sc*CK2$\alpha$ catalytic site, but does not participate in interaction with the regulatory subunits.

## 1. Introduction

Protein phosphorylation is a key regulatory post-translational modification and is involved in the control of many cellular processes. Protein kinase CK2, formerly known as casein kinase 2, which is a highly conserved Ser/Thr/Tyr protein kinase in eukaryotic organisms, plays a central role in a variety of pathways in cell proliferation, transformation, apoptosis and senescence (Allende & Allende, 1995; Montenarh, 2010). Using ATP or GTP as a phosphoryl donor, it can phosphorylate a wide range of proteins involved in the above cellular processes (Pinna, 2002). The phosphorylation target residues

(serine, threonine or tyrosine, referred to as position $p$) of the substrates are often followed by a stretch of acidic amino acids, in particular at the $(p + 1)$ and $(p + 3)$ positions (Meggio & Pinna, 2003). During the reaction, CK2 can use not only the natural cofactor $Mg^{2+}$ ions but also other divalent cations such as $Mn^{2+}$ ions (Niefind *et al.*, 1999).

*Saccharomyces cerevisiae* CK2 (*sc*CK2) is composed of two catalytic subunits, CK2$\alpha$ (44 kDa) and CK2$\alpha'$ (39 kDa), that are expressed by separate genes *CKA1* and *CKA2*, respectively (Glover, 1998). The two isoforms share approximately 60% similarity in their catalytic domains. Disruption of *CKA1* or *CKA2* alone has no effect on cell viability or growth, but simultaneous disruption of both genes is lethal. Studies of temperature-sensitive mutants suggested that *CKA1* plays a greater role in cell-cycle progression, while *CKA2* plays a greater role in cell polarity, and that the two isoforms have different effects on whole genome expression (Berkey & Carlson, 2006). Similar to other lower eukaryotic organisms, *sc*CK2 contains two regulatory subunits, CK2$\beta$ (32 kDa) and CK2$\beta'$ (30 kDa), encoded by the *CKB1* and *CKB2* genes, respectively (Bidwai *et al.*, 1995). In all species tested, the $\beta$ subunits underwent autophosphorylation catalyzed by the $\alpha$ subunits. Whether modification of the $\beta$ subunits serves a regulatory function remains unknown. The sequence of CK2$\beta$, which includes an N-terminal autophosphorylation site, an internal acidic domain and a potential metal-binding motif ($CPX_3CX_{22}CPXC$), displays only 40–45% identity to other $\beta$-subunit sequences reported to date (Reed *et al.*, 1994). *sc*CK2$\beta$ uniquely contains a 30-amino-acid insert. At physiological ionic strength, the $\beta$ subunits stimulate the activity of the $\alpha$ subunits by approximately 5–20-fold against most substrates tested (Antonelli *et al.*, 1996). However, there exist substrates whose phosphorylation is inhibited by $\beta$ subunits, such as calmodulin and MDM-2 (Guerra *et al.*, 1997). Both regulatory subunits CK2$\beta$ and CK2$\beta'$ are indispensable to form an active tetrameric complex in cells as well as *in vitro* reconstitution experiments, and they modulate the substrate specificity and stability of the catalytic subunits. It has been reported that four forms of CK2 exist simultaneously in *S. cerevisiae*: the free catalytic subunit CK2$\alpha'$ and holoenzymes with compositions $\alpha_2\beta\beta'$, $\alpha\alpha'\beta\beta'$ and $\alpha'_2\beta\beta'$. All four isoforms exhibit properties typical of CK2, but differ in substrate specificity as well as in sensitivity to specific modulators (Domańska *et al.*, 2005).

In contrast, mammalian CK2 is isolated as an $\alpha\alpha'\beta_2$, $\alpha_2\beta_2$ or $\alpha'_2\beta_2$ tetramer. The catalytic $\alpha$ subunit of the enzyme is known to exist in three isoforms: CK2$\alpha$, CK2$\alpha'$ and CK2$\alpha''$ (Shi *et al.*, 2001). CK2$\alpha$ and CK2$\alpha'$ are the products of separate genes but demonstrate greater than 90% amino-acid sequence identity over their 330-residue N-terminal part, with unrelated C-terminal sequences (Litchfield, 2003). The CK2$\alpha''$ subunit, which is highly expressed in liver, is nearly identical to CK2$\alpha$ but has a unique sequence of the last 32 amino acids. The regulatory $\beta$-subunit, which is encoded by a single gene in humans, forms a dimer from two identical $\beta$ subunits. Mammalian CK2$\beta$ similarly enhances the stability of catalytic subunits and modulates their substrate specificity.

To date, about 80 released crystal structures of CK2 entities (most of which are CK2$\alpha$ subunits and CK2$\alpha$ subunits coupled with small molecules, with the rest being CK2$\alpha'$ subunits, CK2$\beta$ subunits and holoenzymes) have been deposited in the PDB. The predominant majority of the above structures are of *Zea mays* CK2 (*zm*CK2) and *Homo sapiens* CK2 (*hs*CK2); no structures from *S. cerevisiae* have been reported. The bottleneck in structural research on CK2 is the preparation of protein crystals, owing to its instability. The traditional method of producing crystals remains the vapour-diffusion method, as used for example in the crystallization of CK2$\alpha$ from *Z. mays*. There are also some recent techniques termed 'protein nanocrystallography' that can assist in the crystallization of proteins that resist crystallization attempts using traditionally effective methods (Pechkova & Nicolini, 2004*b*). In addition, nanotechnological approaches appear to be capable of analyzing protein function and protein–protein interaction in studies that are promising for personalized medicine (Nicolini *et al.*, 2012). One of the most impressive example using nanotechnology was the growth of the first crystals of *hs*CK2$\alpha$ using a nanobiofilm template; the crystals diffracted to a maximum resolution of 2.4 Å (PDB entry 1na7; Pechkova & Nicolini, 2002, 2004*a*; Pechkova *et al.*, 2003). CK2 is ubiquitously distributed in eukaryotic organisms, and the amino-acid sequences of the catalytic subunit of CK2 from different species show high similarity. Nevertheless, *sc*CK2$\alpha$ is unique in containing a 38-amino-acid insertion region (Lys93–His130) and the exact function of the insertion region has until now not been interpreted. Here, we present crystal structures of *sc*CK2$\alpha$ with different nucleotides and coordinated divalent cations. These structures reveal multiple nucleotide–divalent cation binding modes of the active site in *sc*CK2$\alpha$, which differ from the two-divalent-cation-occupied catalytic active site of *zm*CK2$\alpha$ or *hs*CK2$\alpha$. A detailed structural comparison presents the structural basis of the abovementioned alternative mechanism. The structural analysis also reveals the structural basis of the dual co-substrate specificity of *sc*CK2$\alpha$ and a probable co-substrate hydrolysis product (ADP/GDP) release pathway. We find that the insertion region does not participate in the interaction with the regulatory subunits of *sc*CK2, but probably contributes to maintaining the constitutively active conformation of *sc*CK2$\alpha$. Our results fill in a gap that has hitherto existed in studies of *sc*CK2$\alpha$, and comprehensive analysis of these crystal structures of *sc*CK2$\alpha$ will be helpful in understanding its catalytic and regulatory mechanisms.

## 2. Materials and methods

### 2.1. Production of recombinant *sc*CK2$\alpha$ and its peptide substrate and of regulatory subunits of *sc*CK2

The full-length DNA fragments for *S. cerevisiae* CK2$\alpha$, CK2$\beta$ and CK2$\beta'$ were amplified from the genomic DNA of *S. cerevisiae* strain S288c by PCR and were then cloned into a modified pET-28a(+) vector with a $His_6$-MBP fusion protein at the N-terminus of the recombinant protein using the *Nde*I and

*Xho*I restriction sites. All of the mutants were generated using two-step PCR and were subcloned, overexpresssed and purified in the same way as the wild-type protein. Overexpression of the recombinant protein was induced in *Escherichia coli* BL21 (DE3) cells (Novagen) with 1 m*M* isopropyl β-D-1-thiogalactopyranoside when the cell density reached an $OD_{600\ nm}$ of 0.8. After 18 h of growth at 16°C, the incubated cells were collected, resuspended in buffer *A* (500 m*M* NaCl, *25* m*M* Tris–HCl pH 7.5) and sonicated. The suspension after centrifugation was applied onto a 5 ml Ni Sepharose Fast Flow column (GE Healthcare) pre-equilibrated with buffer *A*. The bound protein was eluted with buffer *A* containing 500 m*M* imidazole. $His_6$-MBP tags were removed using $His_6$-TEV protease (1 $OD_{280}$ TEV protease per 100 $OD_{280}$ substrate) at 4°C overnight in buffer *A*. This fraction of *sc*CK2α was diluted with buffer *B* (100 m*M* NaCl, 25 m*M* Tris–HCl pH 7.5) and loaded onto a 5 ml HiTrap SP Fast Flow (GE Healthcare) ion-exchange column pre-equilibrated with buffer *B* at 14°C. The *sc*CK2α with extra Gly-His residues at the N-terminus eluted between 300 and 600 m*M* NaCl. After ultrafiltration to 2 ml using a Millipore 10 kDa centrifugal device, the target protein was purified using a Superdex 200 (GE Healthcare) gel-filtration chromatography column previously equilibrated with buffer *A* at 14°C. Finally, the target protein was concentrated to 14 mg $ml^{-1}$ for crystallization trials (calculated from the $OD_{280}$ using a molar absorption coefficient of 71 280 $M^{-1}$ $cm^{-1}$; Eppendorf BioPhotometer Plus). $His_6$-MBP fusion proteins of *sc*CK2β and *sc*CK2β′ digested with $His_6$-TEV protease were concentrated by centrifugal ultrafiltration (Millipore, 10 kDa cutoff) and diluted with buffer *A* until almost no imidazole was present. The proteins were loaded onto a 5 ml column with $Ni^{2+}$–nitrilotriacetate beads. The bound *sc*CK2β and *sc*CK2β′ were eluted with buffer *A* containing 20 m*M* imidazole. The regulatory subunits of *sc*CK2 were then concentrated and eluted from a HiLoad 16/60 Superdex 200 (GE Healthcare) column using buffer *A* at 14°C.

The DNA fragment for the optimum fusion-peptide substrate GST-RRRDDDSDDD-$His_6$ (Kuenzel *et al.*, 1987) was amplified from plasmid pGEX-4T-2 (Novagen) by PCR and was inserted into pET-28a(+) vector (Novagen) using the *Nco*I/*Xho*I restriction sites. The overexpression procedure for the fusion-peptide substrate was similar to that used for *sc*CK2α. The recombinant protein was purified using Ni Sepharose Fast Flow affinity resin at room temperature and a Superdex 200 (GE Healthcare) gel-filtration chromatography column in buffer *A* at 14°C.

### 2.2. Crystallization

Full-length CK2α (amino acids 1–372) and samples with different ligands (the co-substrates ATP and GTP and the co-substrate analogues AMPPNP and GMPPNP) and divalent cations ($Mg^{2+}$ and $Mn^{2+}$) were subjected to crystallization screening using the hanging-drop vapour-diffusion method by equilibrating a drop consisting of 1 µl protein solution and 1 µl reservoir solution against 200 µl reservoir solution at 14°C. Both apo CK2α and the incubated samples yielded crystals, but only crystals of CK2α incubated with ATP–$Mg^{2+}$, AMPPNP–$Mg^{2+}$, GMPPNP–$Mg^{2+}$ and GMPPNP–$Mn^{2+}$ diffracted well enough to allow data collection and processing. CK2α–ATP–$Mg^{2+}$ crystals were obtained using 2 m*M* ATP, 4 m*M* magnesium chloride, 0.2 *M* ammonium sulfate, 20%(*w*/*v*) polyethylene glycol 8000, 0.1 *M* MES pH 6.2, CK2α–AMPPNP–$Mg^{2+}$ crystals were obtained using 2 m*M* AMPPNP, 0.2 *M* magnesium chloride, 25%(*w*/*v*) polyethylene glycol 4000, 0.1 *M* sodium cacodylate pH 6.5, CK2α–GMPPNP–$Mg^{2+}$ crystals were obtained using 2 m*M* GMPPNP, 0.2 *M* magnesium chloride, 25%(*w*/*v*) polyethylene glycol 3350, 0.1 *M* HEPES pH 7.5, and CK2α–GMPPNP–$Mn^{2+}$ crystals were obtained using 2 m*M* GMPPNP, 4 m*M* manganese chloride, 0.2 *M* lithium sulfate monohydrate, 25%(*w*/*v*) polyethylene glycol 3350, 0.1 *M* bis-tris pH 6.5. All crystals grew to maximum size in about 24 h and were cryoprotected in buffer consisting of the corresponding reservoir solution supplemented with 20%(*v*/*v*) glycerol.

### 2.3. Data collection and structure determination

All data were collected on beamline BL17U of Shanghai Synchrotron Radiation Facility (SSRF) and were processed with the *HKL*-2000 package (Otwinowski & Minor, 1997). The *sc*CK2α structures were determined by molecular replacement using *MOLREP* (Vagin & Teplyakov, 2010) from the *CCP*4 suite (Winn *et al.*, 2011). The structure of *hs*CK2α without ligand (PDB entry 1na7; Pechkova *et al.*, 2003), which shows 55% identity to *sc*CK2α, was used as the search model. The initial model from *MOLREP* was refined to the full resolution range using *REFMAC*5 (Murshudov *et al.*, 2011), *PHENIX* (Adams *et al.*, 2010) and manual rebuilding in *Coot* (Emsley & Cowtan, 2004). All structures were checked by *SFCHECK* (Vaguine *et al.*, 1999) and figures were prepared using *PyMOL* (Schrödinger).

### 2.4. Kinetic measurements

The activity test samples had a total volume of 50 µl and contained 0.1 µ*M* *sc*CK2α according to determination of the protein concentration by the UV absorbance method. The other components of the reaction mixture were 500 µ*M* fusion-peptide substrate (GST-RRRDDDSDDD-$His_6$), 15 m*M* $MgCl_2$/$MnCl_2$, 25 m*M* Tris–HCl pH 7.5, 500 m*M* NaCl, 5% glycerol and ATP or GTP at varying concentrations (20–500 µ*M*). After 2 min of incubation at 30°C, the reaction was terminated by heat denaturation at 96°C for 5 min. The supernatant was removed after centrifugation and the precipitate was washed three times with sterile water in order to remove free ATP/GTP, ADP/GDP and phosphate groups. 190 µl buffer (50 m*M* Tris–HCl pH 7.5) and 200 µl 2 *M* NaOH were then added to dissolve the precipitate and the sample tube was incubated for half an hour at 70°C for hydrolysis of the phosphate groups in the phosphorylated protein utilizing hot alkali. It was then left to cool to room temperature, 200 µl 4.7*M* HCl was added to the system and it was centrifuged until the precipitate became pellucid. Finally, 200 µl test solution

**Table 1**
Data-collection and refinement statistics.

Values in parentheses are for the highest resolution shell.

| | CK2$\alpha$–GMPPNP–$Mg^{2+}$ | CK2$\alpha$–ATP–$Mg^{2+}$ | CK2$\alpha$–AMPPN | CK2$\alpha$–GMPPNP–$Mn^{2+}$ |
|---|---|---|---|---|
| Data collection | | | | |
| Resolution range (Å) | 50–1.48 (1.51–1.48) | 50–2.08 (2.15–2.08) | 50–1.80 (1.86–1.80) | 50–1.85 (1.92–1.85) |
| Space group | $P2_12_12_1$ | $P3_221$ | $P2_12_12_1$ | $P3_2$ |
| Wavelength (Å) | 0.9796 | 0.9792 | 0.9792 | 0.9791 |
| Unit-cell parameters (Å, °) | $a$ = 57.74, $b$ = 69.51, $c$ = 94.03, $\beta$ = 90 | $a$ = 69.78, $b$ = 69.78, $c$ = 168.51, $\beta$ = 90 | $a$ = 60.30, $b$ = 69.71, $c$ = 94.56, $\beta$ = 90 | $a$ = 69.66, $b$ = 69.66, $c$ = 166.25, $\beta$ = 90 |
| No. of measured reflections | 441488 | 247542 | 238047 | 558913 |
| No. of unique reflections | 63216 | 29510 | 34615 | 77066 |
| Completeness (%) | 98.7 (85.6) | 99.7 (100) | 91.4 (100) | 99.9 (100) |
| $R_{merge}$† (%) | 6.7 (46.7) | 10.6 (28.3) | 10.8 (44.1) | 7.9 (46.5) |
| Mean $I/\sigma(I)$ | 48.66 (4.13) | 23.65 (14.2) | 16.75 (5.77) | 19.48 (7.75) |
| $V_M$ (Å$^3$ Da$^{-1}$) | 2.25 | 2.83 | 2.37 | 2.78 |
| Refinement statistics | | | | |
| $R_{free}$ | 0.204 | 0.241 | 0.246 | 0.201 |
| $R$ factor | 0.186 | 0.196 | 0.204 | 0.171 |
| Missing residues | Gly−2, His−1, Gly49, Lys50, Tyr51, Pro73, Val74 | Gly−2, His−1, Lys372 | Gly−2, His−1, Met1, Lys2, Lys372 | Gly−2, His−1, Met1, Lys372 |
| Solvent molecules | 259 | 141 | 157 | 501 |
| $B$ factors (Å$^2$) | | | | |
| Protein atoms | 20.697 | 25.919 | 30.645 | 27.35 |
| Nucleotide atoms | 23.221 | 21.639 | 29.137 | 23.74 |
| R.m.s. deviations from ideal | | | | |
| Bond lengths (Å) | 0.008 | 0.010 | 0.018 | 0.008 |
| Bond angles (°) | 1.3 | 1.4 | 1.6 | 1.3 |

† $R_{merge} = \sum_{hkl}\sum_i |I_i(hkl) - \langle I(hkl)\rangle| / \sum_{hkl}\sum_i I_i(hkl)$, where $I_i(hkl)$ is the intensity of an individual reflection and $\langle I(hkl)\rangle$ is the average intensity of that reflection.

from the Phosphoprotein Phosphate Estimation Kit (Sangon Biotech), which contains dye molecules that can combine with free phosphate molecules to form a dye–phosphate complex that has a maximum absorption peak at 620 or 650 nm, was added. 30 min later, the sample was detected at 650 nm to obtain the absorption value, which was proportional to its concentration, using the spectrophotometric method. A standard curve determined from the absorption values of six standard phosphorylated proteins was used for further quantitative analysis. $K_m$ and $V_{max}$ values were determined from Lineweaver–Burk plots and represent the means of three separate assays.

### 2.5. Pull-down assay of regulatory subunits of *sc*CK2 with $His_6$-MBP-*sc*CK2$\alpha$ and $His_6$-MBP-*sc*CK2$\alpha^{\Delta 93-130}$

$His_6$-MBP protein expressed from the modified pET-28a(+) vector used above to express *sc*CK2$\alpha$, *sc*CK2$\beta$ and *sc*CK2$\beta'$ was applied as a negative control. The overexpression and purification of the $His_6$-MBP protein were the same as used for the optimum fusion-peptide substrate of *sc*CK2$\alpha$.

200 µl Ni-affinity resin containing $His_6$-MBP-*sc*CK2$\alpha$, $His_6$-MBP-*sc*CK2$\alpha^{\Delta 93-130}$ or $His_6$-MBP was transferred to three 1.5 ml tubes to which equivalents of purified *sc*CK2$\beta$ and *sc*CK2$\beta'$ were added. The proteins were incubated at 4°C for 30 min and washed three times using buffer *A* containing 50 m*M* imidazole. The Ni-affinity resin was then washed with 400 µl buffer *A* containing 500 m*M* imidazole. The fractions were collected and analyzed by SDS–PAGE.

## 3. Results

### 3.1. Production and kinetics of recombinant *sc*CK2$\alpha$

*sc*CK2$\alpha$ was expressed and purified to greater than 95% homogeneity using affinity chromatography, ion-exchange chromatography and gel-filtration methods. The yield of the protein after purification is approximately 0.8 mg per litre of culture. Although the free catalytic subunit CK2$\alpha$ was not one of the four functional forms of CK2 found in *S. cerevisiae*, the purified recombinant *sc*CK2$\alpha$ was capable of phosphorylating the GST-RRRDDDSDDD-$His_6$ peptide substrate of this kinase (Kuenzel *et al.*, 1987). The $k_{cat}/K_m$ of *sc*CK2$\alpha$ in the presence of ATP–$Mg^{2+}$ and ATP–$Mn^{2+}$ was 0.112 and 0.105 $s^{-1}$ µ$M^{-1}$, respectively, and the $k_{cat}/K_m$ in the presence of GTP–$Mg^{2+}$ and GTP–$Mn^{2+}$ was 0.074 and 0.083 $s^{-1}$ µ$M^{-1}$, respectively. No catalytic activity could be detected without $Mg^{2+}$ or $Mn^{2+}$, indicating that *sc*CK2$\alpha$ appears to be a divalent cation-activated kinase.

### 3.2. Overall structures of *sc*CK2$\alpha$–co-substrate complexes

We determined X-ray structures of *sc*CK2$\alpha$ in complex with ATP–$Mg^{2+}$, with the nonreactive co-substrate analogues guanylyl imidodiphosphate (GMPPNP) with $Mg^{2+}$ and $Mn^{2+}$ and with adenylyl imidodiphosphate (AMPPNP). Four complexes (CK2$\alpha$–ATP–$Mg^{2+}$, CK2$\alpha$–GMPPNP–$Mg^{2+}$, CK2$\alpha$–GMPPNP–$Mn^{2+}$ and CK2$\alpha$–AMPPNP) were refined to 2.08, 1.48, 1.85 and 1.8 Å resolution, respectively, with satisfactory $R$ factors and stereochemical characteristics (Table 1). In the active sites, the co-substrates/analogues were clearly defined by electron density. In the CK2$\alpha$–ATP–$Mg^{2+}$ complex an ATP molecule was identified, but the $\gamma$-phosphate group of

ATP was partially invisible in the electron-density map (Figs. 1*a* and 1*e*). As for the case of ATP, the $\gamma$-phosphate group of GMPPNP in the CK2$\alpha$–GMPPNP–$Mg^{2+}$ complex was partially present in the electron-density map (Figs. 1*b* and 1*f*). Unfortunately, the $\gamma$-phosphate group of AMPPNP could not be modelled because it was totally missing from the electron-density map (Figs. 1*d* and 1*h*). This could be the result of chemical instability, as in a previous report (Ferguson *et al.*, 2011). There are also several unexplained >6$\sigma$ peaks with abnormal shapes or that are distant from other density and we cannot be certain what they represent. These could be noise peaks arising from slight twinning of the crystals. There are also some missing residues (listed in Table 1) and atoms where no corresponding electron-density map is present.

These four complexes reveal high similarity in their overall structures but slight deviations around the co-substrate binding region. They present the classic fold of protein kinase formed by two domains: an N-terminal domain consisting of several $\beta$-sheets and a critical $\alpha$B-helix ($\alpha$C in CK2 from other species and protein kinases), the correct orientation of which is important for catalysis, and a C-terminal domain which is mainly composed of $\alpha$-helices. The co-substrate binding site is located in the cleft between the two domains (Figs. 2*a* and 2*b*). The residues around the cleft showing conservation and diversity contribute to substrate specificity (Cook *et al.*, 2002). Apart from the insertion fragment of *sc*CK2$\alpha$ (Lys93–His130), a strong structural conservation with other CK2$\alpha$ structures is revealed, with r.m.s.d.s of 0.44 Å for 247 $C^{\alpha}$ positions of *sc*CK2$\alpha$–ATP–$Mg^{2+}$ and *zm*CK2$\alpha$–AMPPNP–$Mg^{2+}$ (PDB entry 1daw; Niefind *et al.*, 1999) and of 0.48 Å for 255 $C^{\alpha}$ positions of *sc*CK2$\alpha$–ATP–$Mg^{2+}$ and *hs*CK2$\alpha$–AMPPNP–$Mg^{2+}$ (PDB entry 3u87; Klopffleisch *et al.*, 2012).

## 4. Discussion

### 4.1. The multiple nucleotide–divalent cation binding modes of the active site of *sc*CK2*α*

Most protein kinases contain two divalent cations connecting nonbridging O atoms of ATP/GTP in the active

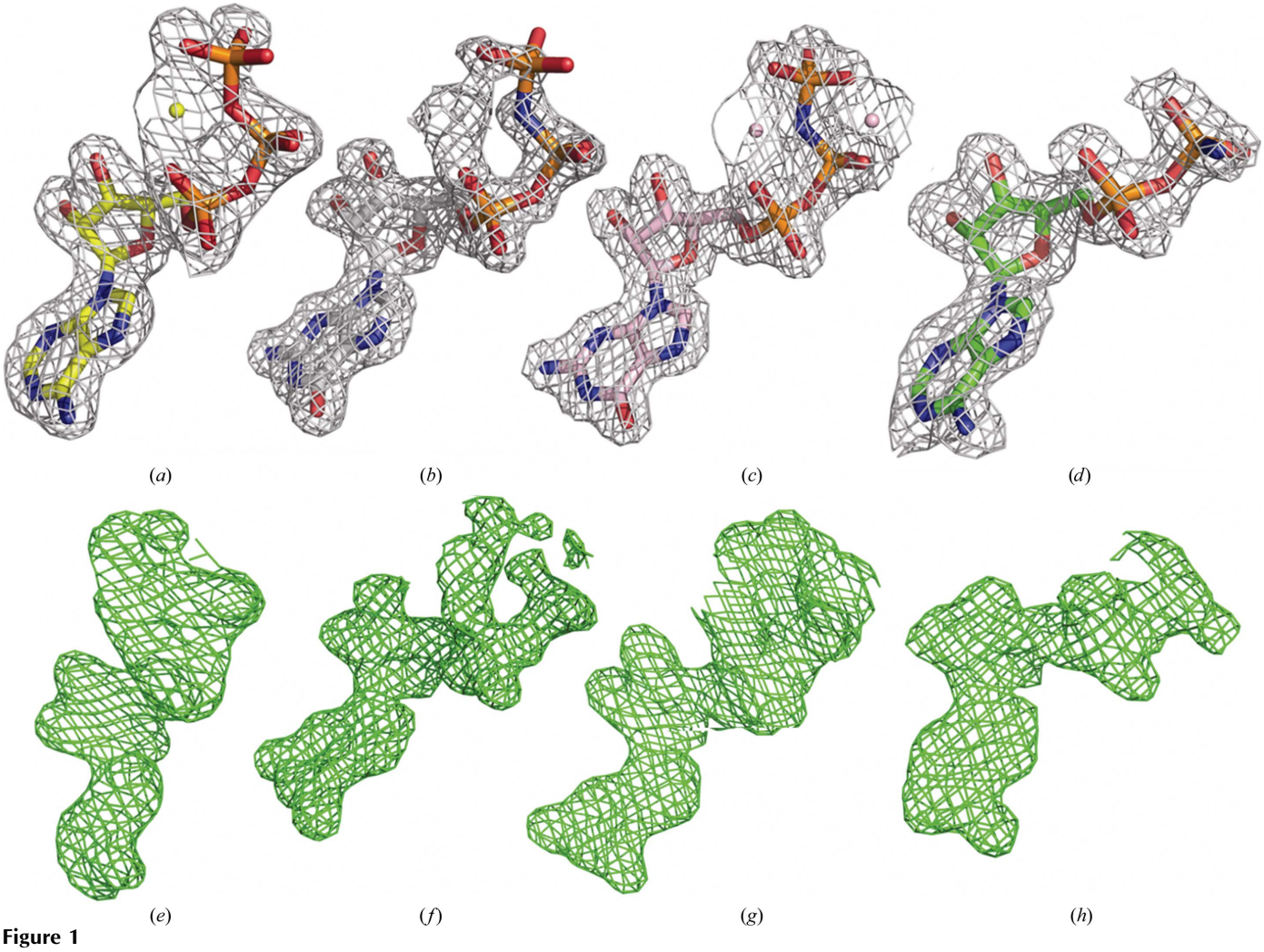


**Figure 1**
The final $2F_o - F_c$ electron-density map (grey, 1$\sigma$ contour level) and the initial and unbiased $F_o - F_c$ electron-density map (green, contoured at 2.5$\sigma$) of the nucleosides and $Mg^{2+}$/$Mn^{2+}$ ions of *sc*CK2$\alpha$ structures: (*a*, *e*) *sc*CK2$\alpha$–ATP–$Mg^{2+}$, (*b*, *f*) *sc*CK2$\alpha$–GMPPNP–$Mg^{2+}$, (*c*, *g*) *sc*CK2$\alpha$–GMPPNP–$Mn^{2+}$, (*d*, *h*) *sc*CK2$\alpha$–AMPPN. Nucleotides and metal ions are shown as sticks and spheres, respectively. The $\gamma$-phosphate group of ATP and GMPPNP can be partially seen in (*a*) and (*b*).

site. The essential cation (which is present in crystals formed at low divalent-cation concentrations) is complexed with nonbridging O atoms of the $\beta$- and $\gamma$-phosphates and is required for catalytic activity. The second cation complexes the $\alpha$- and $\gamma$-phosphates and is present in crystals formed at high divalent-cation concentrations; its role in catalysis is poorly understood, as it has a variety of effects in different protein kinases (Schwartz & Murray, 2011). In the *sc*CK2$\alpha$–GMPPNP–$Mn^{2+}$ structure two ions were determined (Fig. 3*c*), but in the *sc*CK2$\alpha$–ATP–$Mg^{2+}$ and *sc*CK2$\alpha$–GMPPNP–$Mg^{2+}$ structures only one $Mg^{2+}$ ion was identified in the active site even at a high $Mg^{2+}$ concentration (0.2 *M*). In both structures the $Mg^{2+}$ ion contacts the $\alpha$- and $\gamma$-phosphates, corresponding to the second but not the essential divalent cation (Figs. 3*a* and 3*b*). In the structure of *sc*CK2$\alpha$-AMPPN, no $Mg^{2+}$ ion was determined owing to lack of the $\gamma$-phosphate, which could be the result of its release after $\gamma$-phosphate transfer (Fig. 1*d*).

In other CK2$\alpha$–nucleotide complex structures (such as *zm*CK2$\alpha$ complexed with AMPPNP and GMPPNP; PDB entries 1daw and 1day; Niefind *et al.*, 1999) and *hs*CK2$\alpha$ complexed with AMPPNP (PDB entry 3u87; Klopffleisch *et al.*, 2012), the essential divalent cation acts to position the

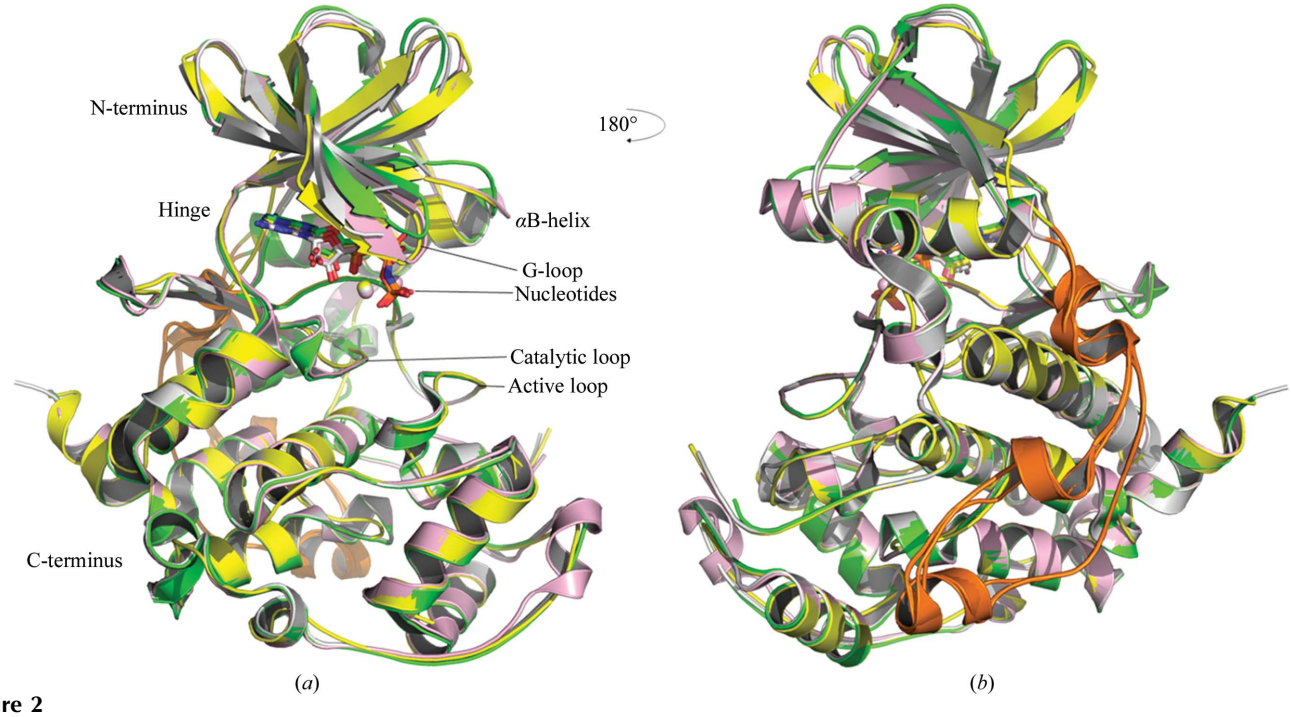


**Figure 2**
Overall structure of *sc*CK2$\alpha$. It contains an N-terminal domain, a C-terminal domain and a substrate-binding pocket between them. The two domains are hinged by a short loop. The N-terminal domain mainly consists of $\beta$-sheets and the important $\alpha$B-helix. The C-terminal domain is composed of $\alpha$-helices. CK2$\alpha$–AMPPN, CK2$\alpha$–ATP–$Mg^{2+}$, CK2$\alpha$–GMPPNP–$Mg^{2+}$ and CK2$\alpha$–GMPPNP–$Mn^{2+}$ are shown in green, yellow, white and pink, respectively. Nucleotides and metal ions are shown as sticks and spheres, respectively. In (*b*), the insertion loop attached to the C-terminal domain of the protein interacting with the N-terminal region is marked in orange.

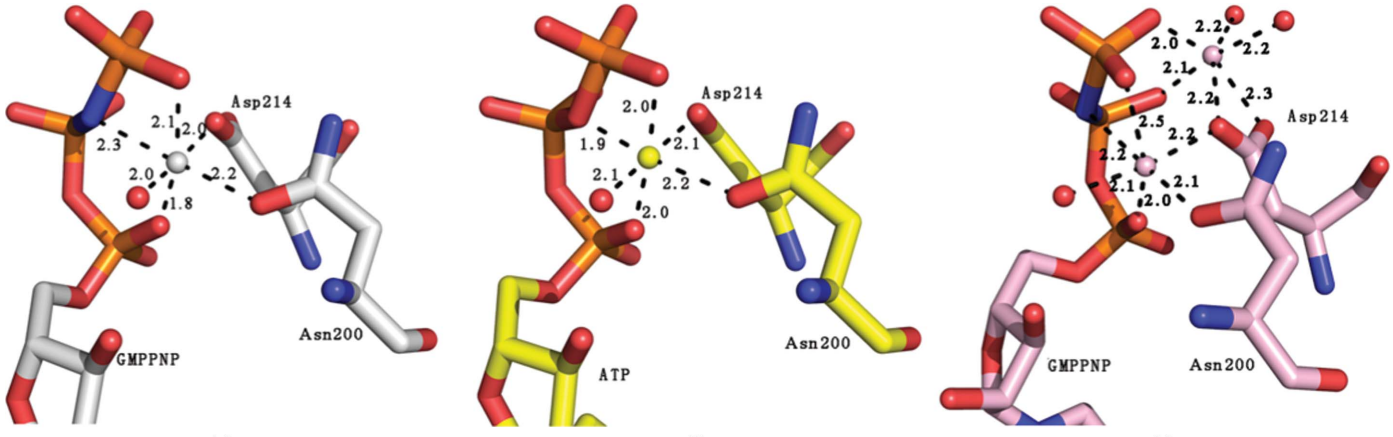


**Figure 3**
Divalent cations in three crystal structures of *sc*CK2$\alpha$. (*a*, *b*) The only $Mg^{2+}$ ion in the co-substrate binding site is coordinated by Asn200 and Asp214, a water molecule and GMPPNP/ATP in the CK2$\alpha$–GMPPNP–$Mg^{2+}$ and CK2$\alpha$–ATP–$Mg^{2+}$ structures. (*c*) The two $Mn^{2+}$ ions in the CK2$\alpha$–GMPPNP–$Mn^{2+}$ structure are coordinated by Asn200 and Asp214, GMPPNP and three water molecules.

$\gamma$-phosphate group of the co-substrate for nucleophilic attack and to mask charge in order to limit charge repulsion with the incoming nucleophile (Adams, 2001). An example of CK2$\alpha$ without a divalent cation is the *hs*CK2$\alpha$ structure (PDB entry 2pvr; Niefind *et al.*, 2007), which was considered to be an inactive state because the $\gamma$-phosphate group of the co-substrate could not be positioned in the correct position to react without coordination by a divalent cation. In contrast, in the *sc*CK2$\alpha$–ATP–$Mg^{2+}$ and *sc*CK2$\alpha$–GMPPNP–$Mg^{2+}$ structures the co-substrate ATP/GMPPNP is fixed in the same position as in the *zm*CK2$\alpha$ and *hs*CK2$\alpha$ complex structures without the essential divalent cation. We aligned the crystal structures of CK2$\alpha$ complexed with metal ions that fix nucleotides in the same active conformation and discovered a conservative residue, Lys50, that adopts a unique conformation in *sc*CK2$\alpha$. In the structures of the *sc*CK2$\alpha$ complexes, one O atom of the $\gamma$-phosphate group of the co-substrate is fixed by a hydrogen bond to the main-chain N atom of Lys50 (the distance between these two atoms is 2.9 Å in *sc*CK2$\alpha$–ATP–$Mg^{2+}$ and 2.8 Å in *sc*CK2$\alpha$–GMPPNP–$Mn^{2+}$; Figs. 4*d* and 4*f*). The $\gamma$-phosphate group of the co-substrate is also fixed by the side chain of Asp214 (Figs. 4*d*, 4*e* and 4*f*). Although Lys50 is conserved among species (Fig. 5), the $\gamma$-phosphate group of the co-substrate is 4.8/5.0 Å from Lys49 of *zm*CK2$\alpha$ and 4.0 Å from Lys49 of *hs*CK2$\alpha$ (the corresponding residue to Lys50 in *sc*CK2$\alpha$; Figs. 4*a*, 4*b* and 4*c*). Owing to the lack of the direct interaction between Lys49 and the $\gamma$-phosphate group, *zm*CK2$\alpha$ and *hs*CK2$\alpha$ may require the essential $Mg^{2+}$ ion to strengthen the interaction between the enzyme and the $\gamma$-phosphate group of the co-substrate. The interaction of the co-substrate with Lys50, Asp214 and the second $Mg^{2+}$ ion is sufficient to fix the $\gamma$-phosphate group of the co-substrate in the correct position, which makes the existence of the essential divalent cation not so essential. It is probable that *sc*CK2$\alpha$ has multiple nucleotide–divalent cation binding modes and that the crystallization experiments happened to capture these different conformations.

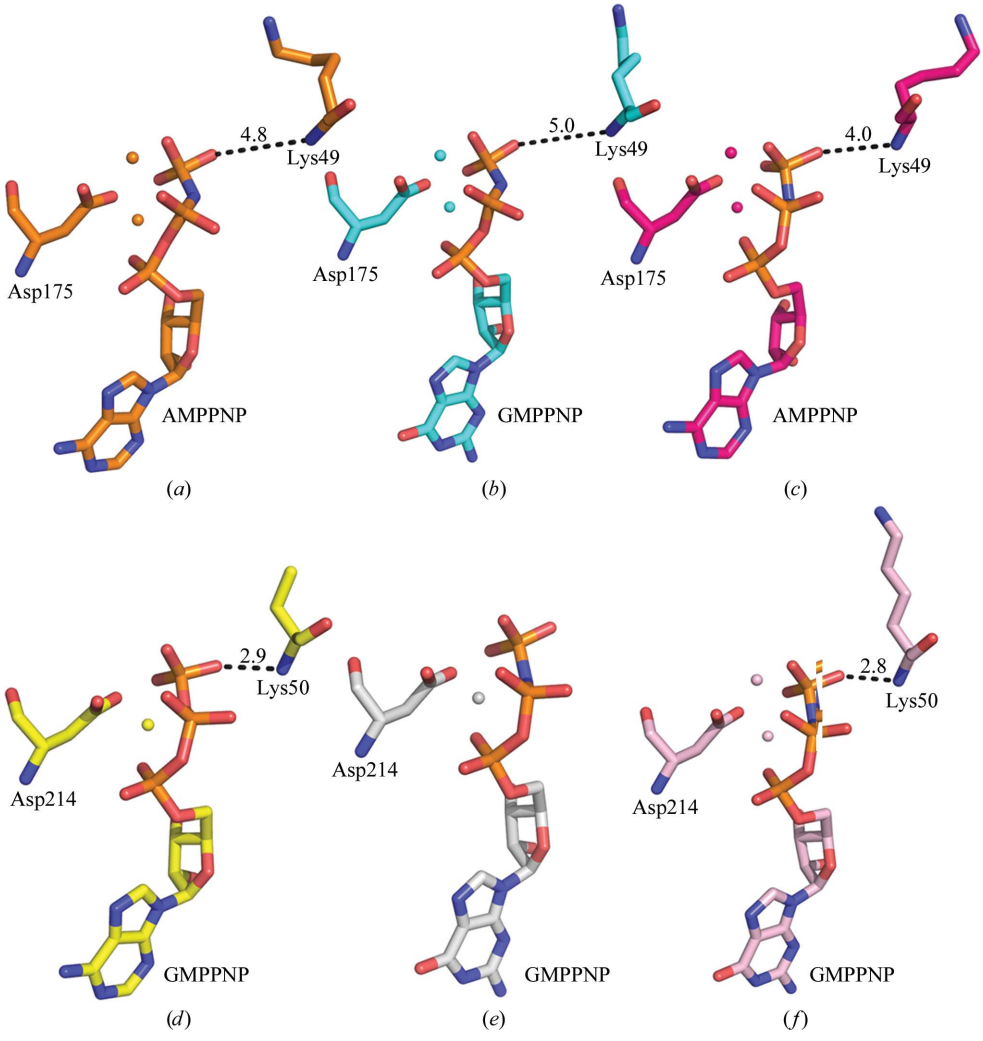


**Figure 4**
The conformation of Lys50 in *sc*CK2$\alpha$ differentiates it from *zm*CK2$\alpha$ and *hs*CK2$\alpha$. (*a*) AMPPNP–$Mg^{2+}$, Lys49 and Asp175 of PDB entry 1daw (*zm*CK2$\alpha$). (*b*) GMPPNP–$Mg^{2+}$, Lys49 and Asp175 of PDB entry 1day (*zm*CK2$\alpha$). (*c*) AMPPNP–$Mg^{2+}$, Lys49 and Asp175 of PDB entry 3u87 (*hs*CK2$\alpha$). (*d*) ATP–$Mg^{2+}$, Lys50 and Asp214 of *sc*CK2$\alpha$ in the CK2$\alpha$–ATP–$Mg^{2+}$ structure. (*e*) GMPPNP–$Mg^{2+}$ and Asp214 of *sc*CK2$\alpha$ in the CK2$\alpha$–GMPPNP–$Mg^{2+}$ structure. (*f*) GMPPNP–$Mn^{2+}$, Lys50 and Asp214 of *sc*CK2$\alpha$ in the CK2$\alpha$–GMPPNP–$Mn^{2+}$ structure.

Alignment analysis demonstrates that three conserved residues, Lys45, Arg48 and Glu53, located in $\beta$1/G-loop/$\beta$2 adopt a different conformation in *sc*CK2$\alpha$ which could result in the unique conformation of Lys50 (Fig. 5). In *sc*CK2$\alpha$–ATP–$Mg^{2+}$ and *sc*CK2$\alpha$–GMPPNP–$Mn^{2+}$, Glu53 interacts with Lys45 and Arg48 through electrostatic interactions (Figs. 6*a* and 6*b*). However, in *zm*CK2$\alpha$–nucleotide and *hs*CK2$\alpha$–nucleotide complexes, Arg47 and Glu52 adopt a more open conformation that makes the Lys44–Glu52 and Arg47–Glu52 distances too great for them to interact with each other (Figs. 6*a*, 6*b* and 6*d*).

In the structure of the *sc*CK2$\alpha$–AMPPN complex, no $Mg^{2+}$ ion was found in the active site. In fact, after transfer of the $\gamma$-phosphate, two coordination bonds formed by the $\gamma$-phosphate and the second $Mg^{2+}$ ion have been eliminated; in addition, the outward swing of AMPPN following $\beta$1/G-loop/$\beta$2 makes the distance between the second $Mg^{2+}$ ion-binding site and Asn200 much greater, which may eliminate the coordination bond

between them (Fig. 7*d*). All of the above changes could lead to the release of the second $Mg^{2+}$ ion from the *sc*CK2$\alpha$–AMPPN complex.

In addition to our study, some other reports have described the catalysis of the protein-phosphorylation process using a divalent-cation-independent mechanism by other enzymes, for example *hs*CASK (Mukherjee *et al.*, 2008) and *hs*STRAD$\alpha$ (Zeqiraj *et al.*, 2009). A mutant of *hs*CASK, *hs*CASK$^{4M}$ (containing G162D, C146N, P22A and H145E mutations), was reported to be capable of transferring the $\gamma$-phosphate using one $Mn^{2+}$ ion (Mukherjee *et al.*, 2010). The above results indicate that the two-divalent-cation-binding mechanism is not the only catalytic mechanism in protein kinases.

### 4.2. A possible release pathway for co-substrate hydrolysis products (ADP/GDP)

The conserved motif Asp-Phe-Gly (DFG) is found in most eukaryotic protein kinase domains adjacent to the ATP-binding site, whereas a Trp replaces the Phe of the DFG motif in CK2$\alpha$ (Shan *et al.*, 2009; Niefind *et al.*, 1998). The previously presented 'DFG-in flip to DFG-out' model indicated that the Asp of the DFG motif potentially binds to the ATP–$Mg^{2+}$ complex and that after phosphate transfer the DFG flip could facilitate ADP release by allowing the kinase to adopt a DFG-out conformation. In CK2$\alpha$, the NE1 atom of Trp in the DWG motif forms a hydrogen bond to the O atom of Leu212, which seems to make the above conformational conversion impossible. This indicates that the ADP-release process of CK2$\alpha$ may differ from the 'DFG-in flip to DFG-out' model.

The three phosphate groups of ATP and GMPPNP are almost at equivalent positions, apart from a slight shift of AMPPN (Fig. 7*e*). The ribose is mainly supported by His199 through a hydrogen bond (ATP/GMPPNP O3′ to His199 O). Asn200 and the $Mg^{2+}$ ion are important in fixing the $\alpha$- and $\gamma$-phosphate groups through an electronic link (Figs. 7*a*, 7*b* and 7*c*). In the CK2$\alpha$–AMPPN structure, because of the shift of AMPPN and $\beta$1/G-loop/$\beta$2, the distance between the ribose and $\alpha$-phosphate group of the nucleotide and the protein becomes too great to form a direct connection. The interaction of the nucleotide with His199 and Asn200 is totally broken and a larger pocket is formed (Figs. 7*d* and 7*e*). A similar phenomenon is found in the case of *hs*CK2$\alpha$ (Fig. 6*d*). It seems that the nucleotide may act as an intermediator linking the

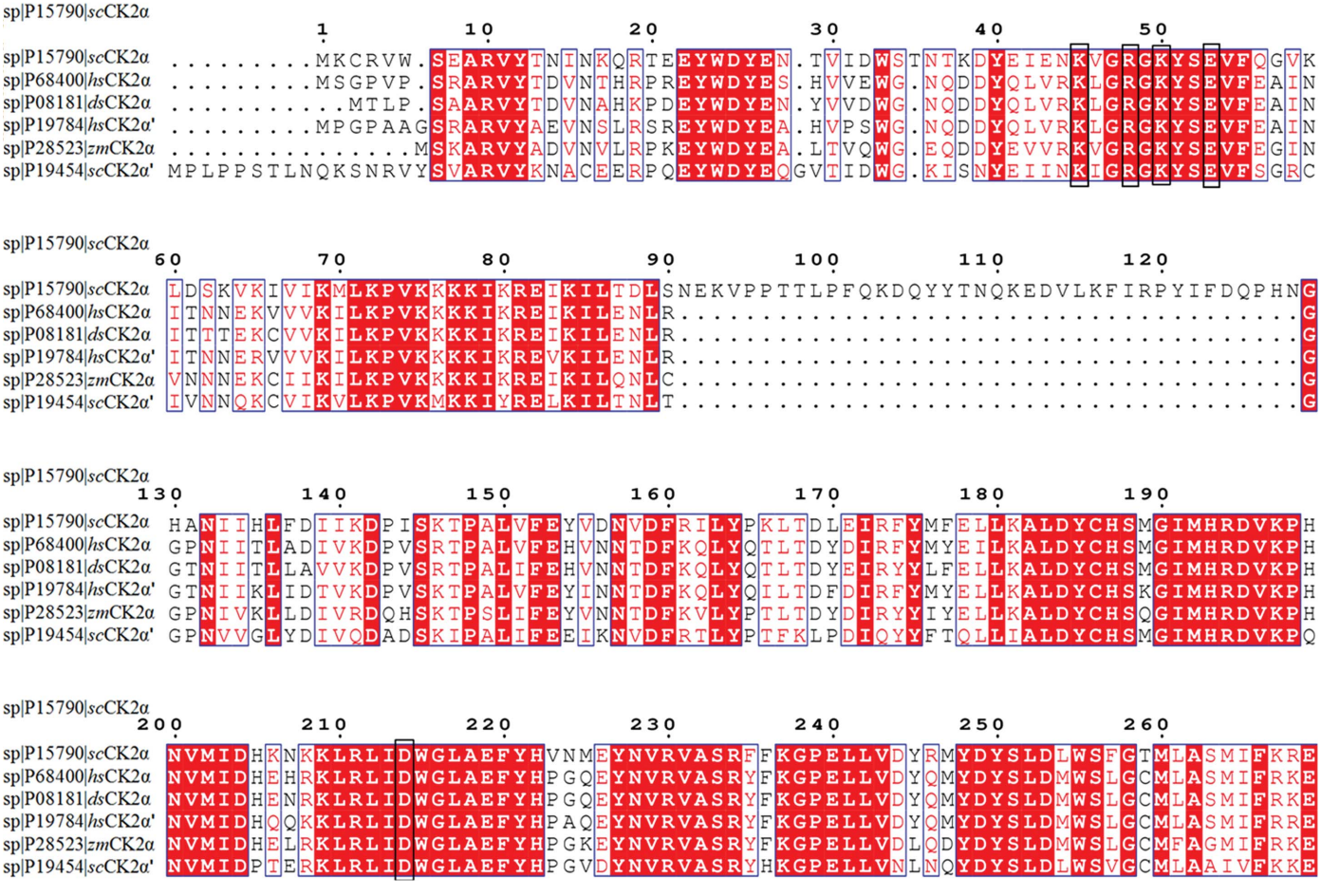


**Figure 5**
Alignment of partial amino-acid sequences of CK2 catalytic subunits from *S. cerevisiae*, *H. sapiens*, *Drosophila melanogaster* and *Z. mays*. The corresponding residues (Lys45, Arg48, Lys50, Glu53 and Asp214) of *sc*CK2$\alpha$ are shown in black boxes.

N-terminal and C-terminal domains of the protein to make the co-substrate binding pocket more compact. Alternatively, after binding of the nucleotide $\beta$1/G-loop/$\beta$2 may move to direct the co-substrate to the proper position. After the hydrolysis of ATP/GTP to ADP/GDP or in the absence of interaction of the $\gamma$-phosphate group with the enzyme, the pocket becomes open. If we think of AMPPN as a product of ATP hydrolysis (ADP), the change in conformation may be a clue to the release of the product ADP/GDP. Thus, we consider that $\beta$1/G-loop/$\beta$2 may act as a gateway to the catalytic pocket; when no co-substrate is present, the cover is open. When the appropriate co-substrate is bound, the cover converts to a closed form and directs the co-substrate to a suitable position to start the catalytic process. During the release of ADP/GDP, the pocket may become open again because of movement of $\beta$1/G-loop/$\beta$2. Unfortunately, we did not obtain a high-resolution structure of *sc*CK2$\alpha$ without nucleotide to support the above opinion, but we clearly observed a larger co-substrate binding pocket to form when *sc*CK2$\alpha$ was coupled with AMPPN (which can be seen as the ATP hydrolysis product ADP) compared with when *sc*CK2$\alpha$ was coupled with ATP. This indicates that when ATP/GTP is hydrolysed to ADP/GDP, $\beta$1/G-loop/$\beta$2 of *sc*CK2$\alpha$ would perform a conformation change to facilitate the release of the hydrolysis product.

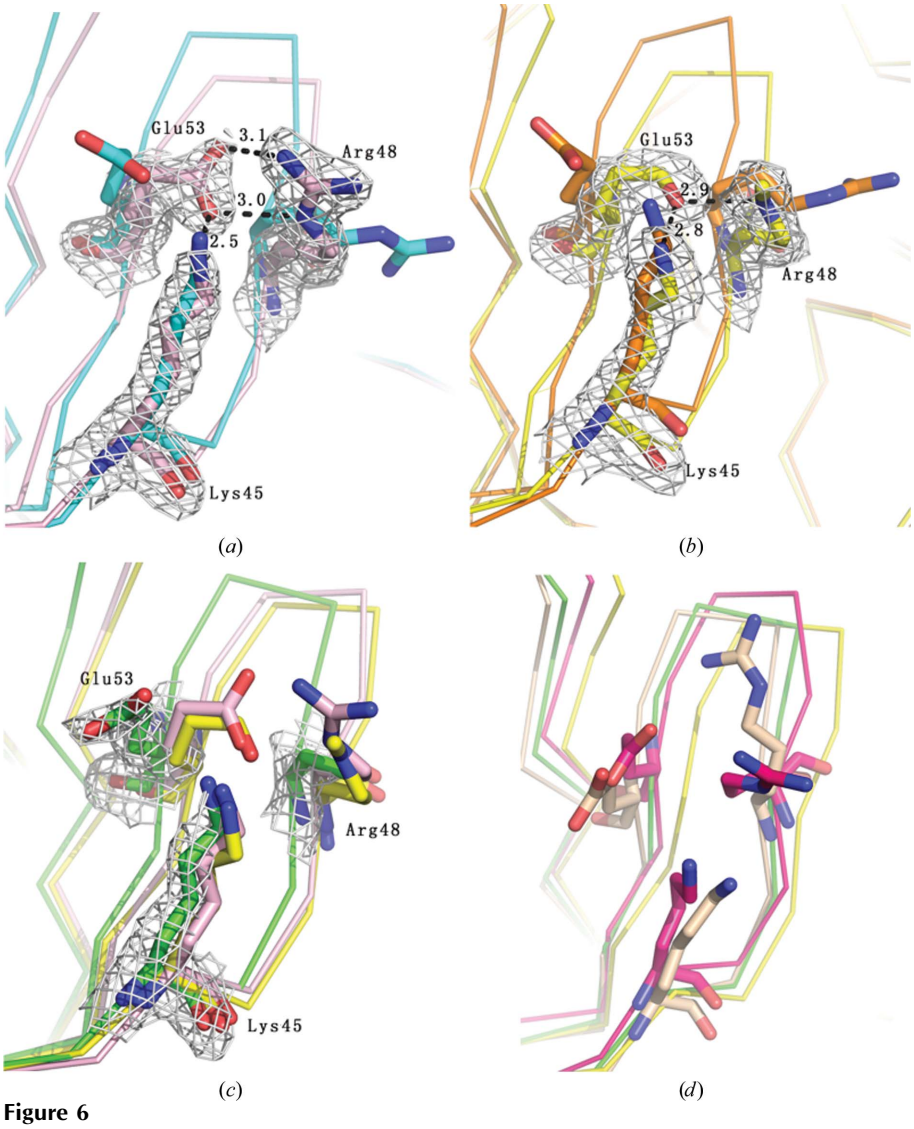


**Figure 6**
The conformation and interaction of Lys45, Arg48 and Glu53 in *sc*CK2$\alpha$ may be the cause of the unique conformation of Lys50 and the more open conformation of $\beta$1/G-loop/$\beta$2 during ADP/GDP release. (*a*, *b*) In *sc*CK2$\alpha$–GMPPNP–$Mn^{2+}$ (pink) and *sc*CK2$\alpha$–ATP–$Mg^{2+}$ (yellow), Glu53 interacts with Lys45 and Arg48 through electrostatic interactions and the final $2F_o - F_c$electron-density maps (grey, 1$\sigma$ contour level) are presented for the three residues. In contrast, in *zm*CK2$\alpha$, PDB entries 1day (*a*) (cyan) and 1daw (*b*) (orange), Arg47 and Glu52 adopt a more open conformation that makes the Lys44–Arg47 and Lys44–Glu52 distances too large for these residues to interact with each other. (*c*) In *sc*CK2$\alpha$–AMPPN, Glu53 adopts an obviously different conformation compared with Glu53 in *sc*CK2$\alpha$–ATP–$Mg^{2+}$ and *sc*CK2$\alpha$–GMPPNP–$Mn^{2+}$, which makes interaction with Lys45 and Arg48 impossible. (*d*) In *hs*CK2$\alpha$–nucleotide complexes (*hs*CK2$\alpha$–AMPPNP–$Mg^{2+}$, PDB entry 3u87, hot pink; *hs*CK2$\alpha$–AMPPN–$Mg^{2+}$, PDB entry 3nsz, wheat), Lys44, Arg47 and Glu52 adopt a more open conformation, which is similar to that in *sc*CK2$\alpha$–AMPPN. Both *sc*CK2$\alpha$–AMPPN and PDB entry 3nsz adopt a more open conformation compared with *sc*CK2$\alpha$–ATP–$Mg^{2+}$ and PDB entry 3u87, which contain nucleotides with three phosphate groups.

The residues Lys45, Arg48 and Glu53 referred to above may be possible factors affecting the size of the gateway of the active site. We could not detect electron density for the side chain of Arg48 in *sc*CK2$\alpha$–AMPPN, but Glu53 adopts an obviously different conformation compared with Glu53 in *sc*CK2$\alpha$–ATP–$Mg^{2+}$ and scCK2$\alpha$–GMPPNP–$Mn^{2+}$, which makes its interaction with Lys45 and Arg48 impossible. However, the conformation of Glu53 is similar to that of Glu52 of *zm*CK2$\alpha$ and *hs*CK2$\alpha$, which have a lager gateway (Figs. 6*c* and 6*d*).

In the structures of *sc*CK2$\alpha$–ATP–$Mg^{2+}$ and *sc*CK2$\alpha$–GMPPNP–$Mn^{2+}$, we identified some sulfate ions on the basic surface of the protein owing to the presence of 0.2 *M* sulfate in the crystallization solution (Figs. 8*a* and 8*b*). Two of these, which were located around the co-substrate binding pocket and were bound to Arg161 and Lys197, caught our attention (purple sticks in Fig. 8*a*). We hold the opinion that the two sulfate ions around the co-substrate binding pocket may mimic two phosphate groups, indicating a potential ATP/ADP-binding/release pathway in *sc*CK2$\alpha$. Biochemical experiments using the R161A and K197A mutants indicate that these mutants show an obvious reduction in catalytic efficiency and affinity for ATP (Figs. 8*c* and 8*d*). This supports our opinion that these two positions are important in the ATP-

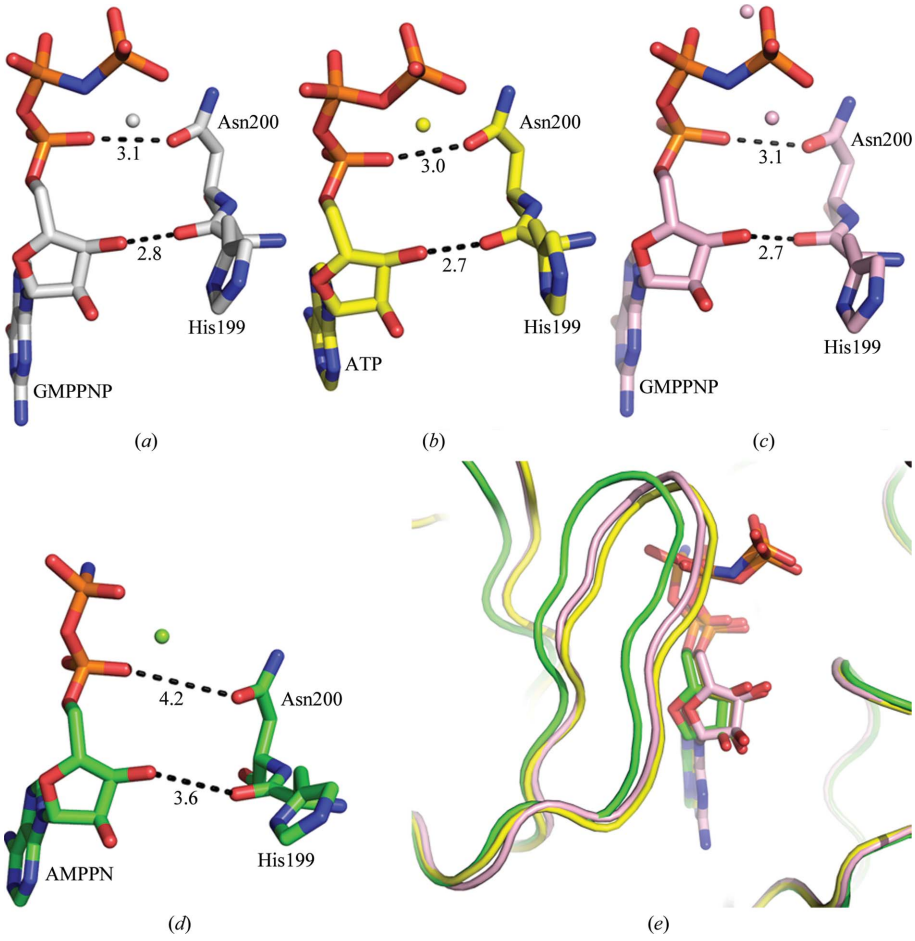


**Figure 7**
Interaction of His199 and Asn200 with nucleotides. (*a*, *b*, *c*) The riboses and α-phosphate groups of the nucleotides are stabilized by Asn200 and His199. (*d*) The distance between the ribose and α-phosphate group of AMPPN and residues Asn200 and His199 is too far to form a direct linkage. (*e*) Alignment of the nucleotide-binding region (β1/G-loop/β2) of CK2α–ATP–$Mg^{2+}$ (yellow), CK2α–GMPPNP–$Mn^{2+}$ (pink) and CK2α–AMPPN (green).

binding process of *sc*CK2α and also corresponds with our conjecture above.

### 4.3. The insertion loop maintains a more stable open conformation of the *sc*CK2α active site

The amino-acid sequence alignment of CK2 catalytic subunits from *S. cerevisiae* and other species demonstrates that *sc*CK2α is unique by containing an extra 38-amino-acid insertion sequence (Lys93–His130; Padmanabha *et al.*, 1990; Fig. 5). A previous report modelled the structure of *sc*CK2α and predicted that this extra region forms two α-helical structures and extends out over the protein surface (Sajnaga *et al.*, 2008). Our crystal structures reveal that it is a long insertion loop consisting of four short α-helices linking the αB-helix and β4 and is located far away from the active site even though they are close in the primary sequence. It lies on the surface of the C-terminal domain of the protein and its orientation parallels that of the N-terminal loop (Fig. 9*b*). Considering the area that it crosses, this insertion loop may provide a platform for

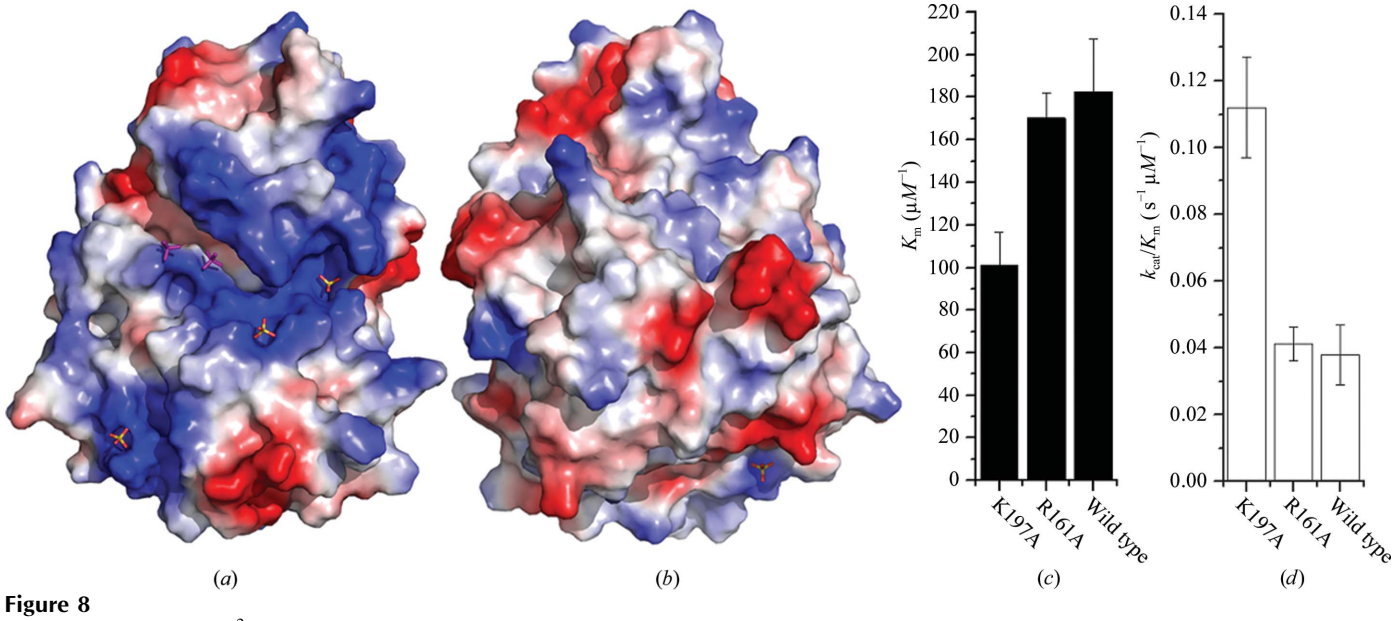


**Figure 8**
(*a*, *b*) In CK2α–ATP–$Mg^{2+}$, six sulfate ions were identified on the basic surface of the protein, two of which (purple sticks) are located around the co-substrate binding pocket and are captured by Arg161 and Lys197. (*c*, *d*) Kinetic parameters ($K_m$ and $k_{cat}/K_m$) of wild-type *sc*CK2α and two mutants, R161A and K197A, calculated in the presence of ATP and 15 m*M* $MgCl_2$.

protein–protein interaction. To verify whether the loop interacts with the regulatory subunits, a pull-down assay was carried out. The result suggested that the insertion loop does not participate in interaction with regulatory subunits (Fig. 9*c*). This result is coincident with the crystal structure of the *hs*CK2 holoenzyme (PDB entry 1jwh; Niefind *et al.*, 2001), in which the corresponding position of the insertion loop of *sc*CK2$\alpha$ is distant from the interface of the catalytic and regulatory subunits (Fig. 9*d*).

At variance with the great majority of protein kinases, which only become active in response to specific stimuli, the highly pleiotropic Ser/Thr/Tyr-specific protein kinase CK2 is constitutively active under normal conditions (Niefind *et al.*, 1999). It is acknowledged that the existence of the N-terminal loop connected to the active loop contributes to the open conformation of the active site, which makes substrate access and product release easy and is the cause of the enzyme maintaining its activity at all times without regulation (Niefind *et al.*, 1998). In the case of *sc*CK2$\alpha$, the active loop (Ile213–Gly238) is fixed by the N-terminal loop (Ser7–Asn36), the basic cluster (Lys75–Arg81) of the $\alpha$B-helix and some other residues of the C-terminal domain, which stabilize the open conformation of the active site. The $\alpha$B-helix interacts with the active loop through a hydrogen bond (Arg81 N to Glu219 OE1). The N-terminal loop simultaneously interacts with the active loop (through hydrogen bonds: Ala9 N to Tyr221 OH, Asn16 ND2 to Tyr221 O and Tyr26 OH to Glu219 OE1) and the $\alpha$B-helix (through a hydrogen bond from Glu27 O to Lys80 NZ; Fig. 9*a*). In addition, the insertion loop contacts the N-terminal loop through an electrovalent bond (Arg19 to Glu92) and hydrogen bonds (Glu109 ND2 to Ala9 O and Glu8 O, Arg10 O to Thr108 N and Asn109 N, Thr108 OG1 to Thr13 OG1, Thr13 N and Tyr12 N, and Tyr106 O to Tyr12 N) (Fig. 9*b*). These interactions may

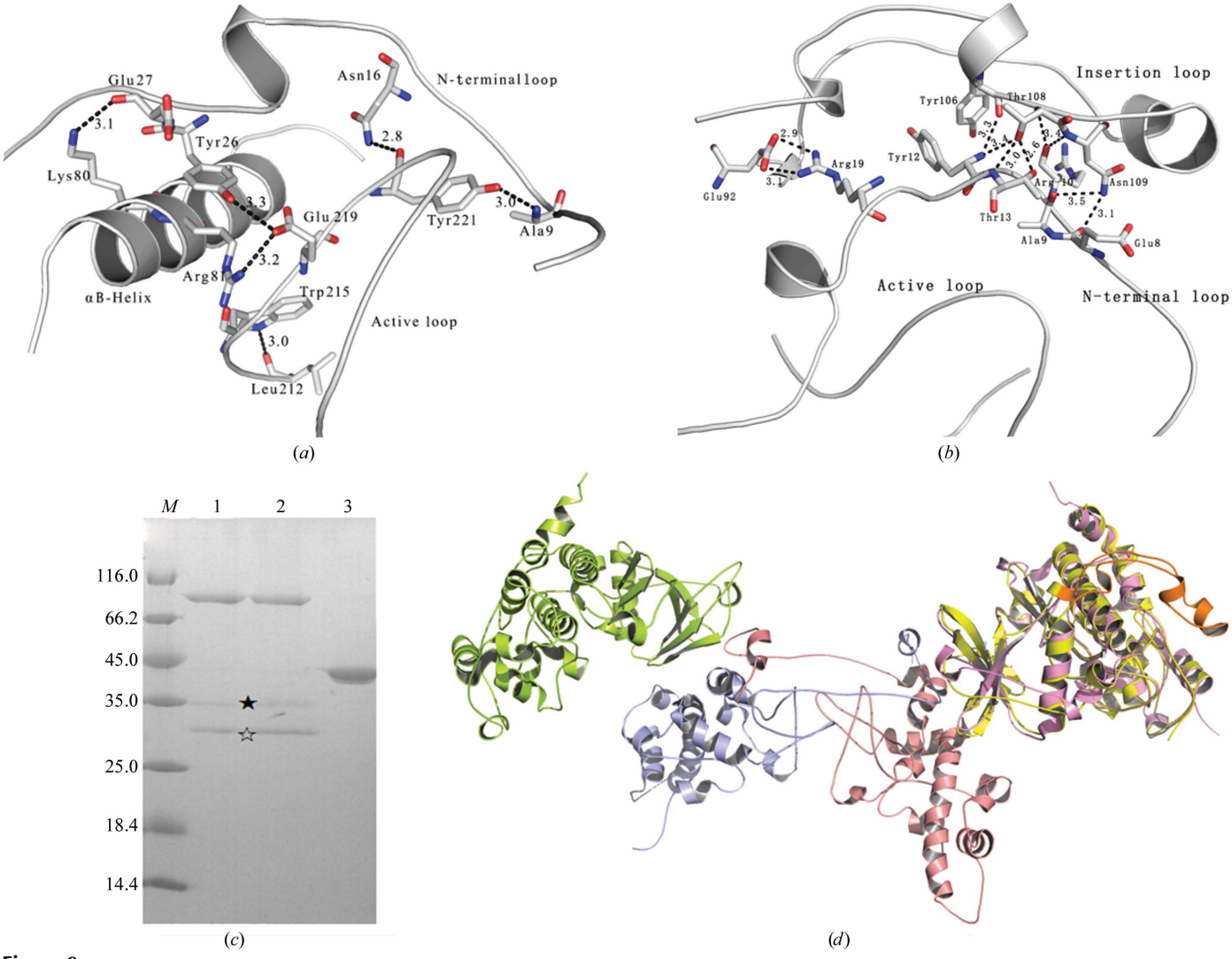


**Figure 9**
Interaction of the N-terminal loop, insertion loop and active loop. (*a*) The N-terminal loop, active loop and $\alpha$B-helix interact with each other. (*b*) Interaction of the N-terminal loop with the insertion loop. (*c*) Pull-down assay of the regulatory subunits of *sc*CK2 with $His_6$-MBP-*sc*CK2$\alpha$ and $His_6$-MBP-*sc*CK2$\alpha^{\Delta 93-130}$. Lane *M*, marker (labelled in kDa). Lane 1, $His_6$-MBP-*sc*CK2$\alpha$ + *sc*CK2$\beta$ (filled star) + *sc*CK2$\beta'$ (empty star). Lane 2, $His_6$-MBP-*sc*CK2$\alpha^{\Delta 93-130}$ + *sc*CK2$\beta$ (filled star) + *sc*CK2$\beta'$ (empty star). Lane 3, $His_6$-MBP. (*d*) Alignment of PDB entry 1jwh with CK2$\alpha$–ATP–$Mg^{2+}$ (yellow), in which the insertion loop is marked in orange.

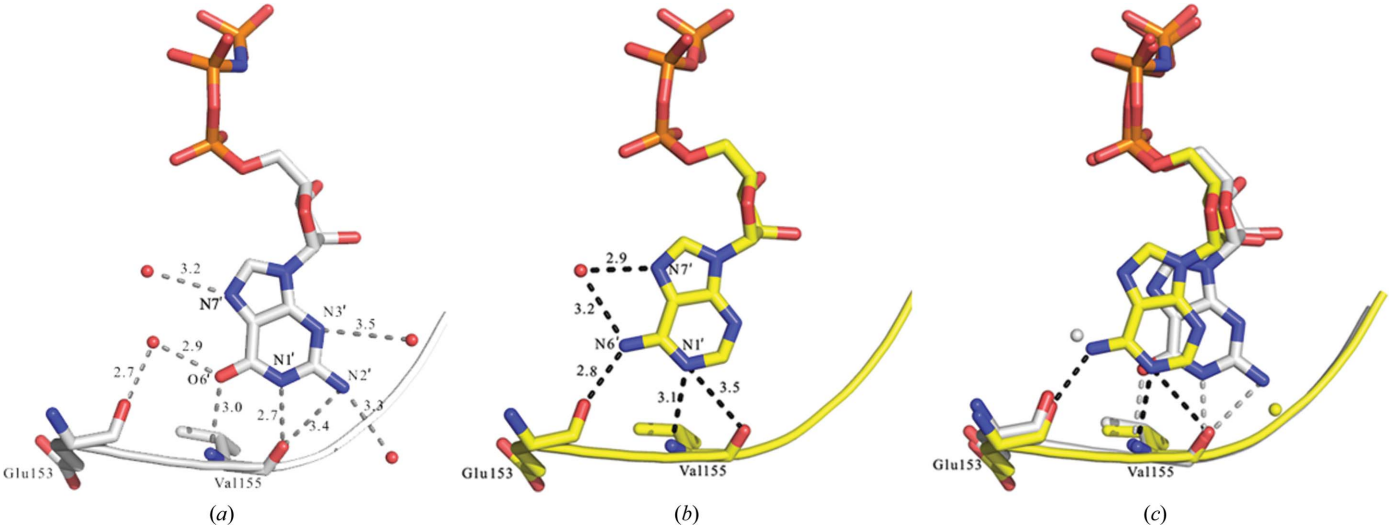


**Figure 10**
Structural basis of the dual nucleotide selectivity. (*a*) In CK2$\alpha$–GMPPNP–$Mg^{2+}$, the purine base of guanine is fixed by Glu153 and Val155 of the protein and several water molecules. (*b*) In CK2$\alpha$–ATP–$Mg^{2+}$, the purine base of adenine is fixed by the hinge region of the protein and a water molecule. (*c*) Alignment of CK2$\alpha$–ATP–$Mg^{2+}$ and CK2$\alpha$–GMPPNP–$Mg^{2+}$ shows two different hydrogen-bonding patterns and the relative positions of two different nucleotides.

consolidate the rigidity of the N-terminal loop and its connection to the active loop and enhance the stability of the open conformation of the active site. Previous research indicated that deletion of the 38-amino-acid insertion loop from *sc*CK2$\alpha$ decreased its catalytic efficiency (Sajnaga *et al.*, 2008). As the insertion loop does not directly participate in the catalytic process, the most probable reason for this decrease in catalytic efficiency may be that the lack of the 38-amino-acid insertion loop influences the open active-site conformation of *sc*CK2$\alpha$.

### 4.4. The structural basis of the dual co-substrate specificity of *sc*CK2*α*

CK2 is a prime example of dual co-substrate specificity. In contrast to most other protein kinases, CK2 and CK2$\alpha$ from all sources efficiently utilize ATP or GTP as phosphoryl donors (Niefind *et al.*, 1999). As in all other well defined three-dimensional structures of protein kinases complexed with ATP or GTP in the PDB, the nucleotides in the *sc*CK2$\alpha$ structures are entirely buried in the co-substrate binding pocket. The purine base of the nucleotide is supported by the amide backbone of the hinge region between the two domains through hydrogen bonds in a strictly conserved way. Glu153 O and Val155 N in the protein are the hydrogen-bonding partners of the N6′ and N1′ atoms of adenine, respectively. N6′ and N7′ are also hydrogen bonded to a water molecule (Fig. 10*b*). In the case of guanine, Val155 N and Val155 O interact with O6′ and N1′ of the guanine base *via* a hydrogen bond. Some water molecules also participate in the connection between O6′, N2′ and N7′ (Fig. 10*a*). As the hydrogen-bond acceptor, the N1′ atom of adenine and the O6′ atom of guanine are almost in the same position, interacting with the hydrogen-bond donor Val155 N. N6′ of adenine and N1′ of guanine, which act as hydrogen donors, interact with Glu153 O and Val155 O, respectively. This leads to the observation of two different hydrogen-bonding patterns, as in previous research on *zm*CK2$\alpha$ (Niefind *et al.*, 1999).

The mechanism by which CK2$\alpha$ overcomes restrictions to use both GTP and ATP *via* a hydrogen-bonding frame-shift has been presented in detail by Niefind *et al.* (1999). Consistent with the above mechanism, the backbone of the *sc*CK2$\alpha$ hinge region shows approximate $\beta$-strand geometry and thus alternately provides hydrogen donors and acceptors. Consequently, the guanine base is displaced relative to the position of adenine along the backbone until the hydrogen-bond donors and acceptors match up again correctly. The hydrogen-bonding frame-shift leaves a gap at the position of the N6′ atom of adenine. This gap is filled with a water molecule, which in combination with Glu153 mimics the hydrogen-bonding potential of adenine. Likewise, in the structure of the CK2$\alpha$–ATP–$Mg^{2+}$ complex a water molecule occupies the position of the N2′ atom of GMPPNP (Fig. 10*c*).

We are grateful to the staff members at SSRF for the collection of diffraction data. Financial support for this project was provided by the Chinese Ministry of Science and Technology (Grant Nos. 2012CB917200 and 2009CB825500) and the Chinese National Natural Science Foundation (Grant Nos. 31270014, 31130018, 30900224 and 10979039).

## References

Adams, J. A. (2001). *Chem. Rev.* **101**, 2271–2290.
Adams, P. D. *et al.* (2010). *Acta Cryst.* D**66**, 213–221.
Allende, J. E. & Allende, C. C. (1995). *FASEB J.* **9**, 313–323.
Antonelli, M., Daniotti, J. L., Rojo, D., Allende, C. C. & Allende, J. E. (1996). *Eur. J. Biochem.* **241**, 272–279.
Berkey, C. D. & Carlson, M. (2006). *Curr. Genet.* **50**, 1–10.
Bidwai, A. P., Reed, J. C. & Glover, C. V. (1995). *J. Biol. Chem.* **270**, 10395–10404.

Cook, A., Lowe, E. D., Chrysina, E. D., Skamnaki, V. T., Oikonomakos, N. G. & Johnson, L. N. (2002). *Biochemistry*, **41**, 7301–7311.
Domańska, K., Zieliński, R., Kubiński, K., Sajnaga, E., Masłyk, M., Bretner, M. & Szyszka, R. (2005). *Acta Biochim. Pol.* **52**, 947–951.
Emsley, P. & Cowtan, K. (2004). *Acta Cryst.* D**60**, 2126–2132.
Ferguson, A. D., Sheth, P. R., Basso, A. D., Paliwal, S., Gray, K., Fischmann, T. O. & Le, H. V. (2011). *FEBS Lett.* **585**, 104–110.
Glover, C. V. III (1998). *Prog. Nucleic Acid Res. Mol. Biol.* **59**, 95–133.
Guerra, B., Götz, C., Wagner, P., Montenarh, M. & Issinger, O.-G. (1997). *Oncogene*, **14**, 2683–2688.
Klopffleisch, K., Issinger, O.-G. & Niefind, K. (2012). *Acta Cryst.* D**68**, 883–892.
Kuenzel, E. A., Mulligan, J. A., Sommercorn, J. & Krebs, E. G. (1987). *J. Biol. Chem.* **262**, 9136–9140.
Litchfield, D. W. (2003). *Biochem. J.* **369**, 1–15.
Meggio, F. & Pinna, L. A. (2003). *FASEB J.* **17**, 349–368.
Montenarh, M. (2010). *Cell Tissue Res.* **342**, 139–146.
Mukherjee, K., Sharma, M., Jahn, R., Wahl, M. C. & Sudhof, T. C. (2010). *Sci. Signal.* **3**, ra33.
Mukherjee, K., Sharma, M., Urlaub, H., Bourenkov, G. P., Jahn, R., Südhof, T. C. & Wahl, M. C. (2008). *Cell*, **133**, 328–339.
Murshudov, G. N., Skubák, P., Lebedev, A. A., Pannu, N. S., Steiner, R. A., Nicholls, R. A., Winn, M. D., Long, F. & Vagin, A. A. (2011). *Acta Cryst.* D**67**, 355–367.
Nicolini, C., Bragazzi, N. & Pechkova, E. (2012). *Adv. Drug Deliv. Rev.* **64**, 1522–1531.
Niefind, K., Guerra, B., Ermakowa, I. & Issinger, O.-G. (2001). *EMBO J.* **20**, 5320–5331.
Niefind, K., Guerra, B., Pinna, L. A., Issinger, O.-G. & Schomburg, D. (1998). *EMBO J.* **17**, 2451–2462.
Niefind, K., Pütter, M., Guerra, B., Issinger, O.-G. & Schomburg, D. (1999). *Nature Struct. Biol.* **6**, 1100–1103.
Niefind, K., Yde, C. W., Ermakova, I. & Issinger, O.-G. (2007). *J. Mol. Biol.* **370**, 427–438.
Otwinowski, Z. & Minor, W. (1997). *Methods Enzymol.* **276**, 307–326.
Padmanabha, R., Chen-Wu, J. L.-P., Hanna, D. E. & Glover, C. V. (1990). *Mol. Cell. Biol.* **10**, 4089–4099.
Pechkova, E. & Nicolini, C. (2002). *J. Cell. Biochem.* **85**, 243–251.
Pechkova, E. & Nicolini, C. (2004*a*). *J. Cell. Biochem.* **91**, 1010–1020.
Pechkova, E. & Nicolini, C. (2004*b*). *Trends Biotechnol.* **22**, 117–122.
Pechkova, E., Zanotti, G. & Nicolini, C. (2003). *Acta Cryst.* D**59**, 2133–2139.
Pinna, L. A. (2002). *J. Cell Sci.* **115**, 3873–3878.
Reed, J. C., Bidwai, A. P. & Glover, C. V. (1994). *J. Biol. Chem.* **269**, 18192–18200.
Sajnaga, E., Kubiński, K. & Szyszka, R. (2008). *Acta Biochim. Pol.* **55**, 767–776.
Schwartz, P. A. & Murray, B. W. (2011). *Bioorg. Chem.* **39**, 192–210.
Shan, Y., Seeliger, M. A., Eastwood, M. P., Frank, F., Xu, H., Jensen, M. Ø., Dror, R. O., Kuriyan, J. & Shaw, D. E. (2009). *Proc. Natl Acad. Sci. USA*, **106**, 139–144.
Shi, X., Potvin, B., Huang, T., Hilgard, P., Spray, D. C., Suadicani, S. O., Wolkoff, A. W., Stanley, P. & Stockert, R. J. (2001). *J. Biol. Chem.* **276**, 2075–2082.
Vagin, A. & Teplyakov, A. (2010). *Acta Cryst.* D**66**, 22–25.
Vaguine, A. A., Richelle, J. & Wodak, S. J. (1999). *Acta Cryst.* D**55**, 191–205.
Winn, M. D. *et al.* (2011). *Acta Cryst.* D**67**, 235–242.
Zeqiraj, E., Filippi, B. M., Goldie, S., Navratilova, I., Boudeau, J., Deak, M., Alessi, D. R. & van Aalten, D. M. F. (2009). *PLoS Biol.* **7**, e1000126.